Int. J. Open Problems Compt. Math., Vol. 19, No. 2, June 2026
Print ISSN: 1998-6262, Online ISSN: 2079-0376

GATE Monte Carlo Simulation of the RS 3400 X-ray Blood Irradiator: Dose Distribution Analysis in a MAGIC-f Gel Blood-Bag Phantom

Ahmed S. Aljuhani[1], Fathi Djouider[2], and Ahmad Yahya[3]
[1,2,3]*Nuclear Engineering Department, Faculty of Engineering, King Abdulaziz University, Jeddah, Saudi Arabia*
e-mail: assaljuhani1@kau.edu.sa

Received 4 March 2026; Accepted 22 May 2026

Abstract

Accurate spatial dose verification is essential for ensuring the reliability of compact X-ray blood irradiators used to prevent transfusion-associated graft-versus-host disease. This work develops and characterizes a Monte Carlo dosimetric model of the RS 3400 self-contained X-ray blood irradiator operating at 150 kV / 10 mA for a 280 s protocol, using the GATE v9.0 toolkit built on Geant4. The model reproduces the gold-anode 150 kV X-ray spectrum, a seven-component lead-shielding assembly, an ellipsoidal MAGIC-f polymer-gel blood-bag phantom, and the combined self-rotation (6°/s) and orbital revolution (3°/s) of the sample, discretized into 28 000 time slices over the irradiation period with 10^{10} primary photons tracked. A unified MATLAB post-processing pipeline converts the energy-deposition output to absorbed dose and performs voxel-wise uncertainty, regional, inner-subregion, and ROI-based analyses in the coronal plane. The simulated distribution exhibits a homogeneous central plateau (inner-region mean 23.92 Gy, uniformity ratio 1.08) that decreases radially toward the periphery, with a mean voxel-wise statistical uncertainty of 0.771 %. The results confirm that the combined motion model effectively homogenizes the central dose and that the model is converged to a clinically useful precision.

Keywords: Absorbed dose, Blood irradiator, Dose uniformity, GATE Monte Carlo, RS 3400, X-ray spectrum.

1 Introduction

Accurate dosimetry in blood irradiation systems is essential to ensure uniform dose delivery across all blood product components while avoiding over-irradiation that could compromise cellular function or under-irradiation that might leave viable lymphocytes could survive and cause TA-GVHD. Irradiate too much, and you risk damaging the blood components themselves. Regulations typically mandate minimum doses of 25 Gy with no portion receiving less than 15 Gy or more than 50 Gy [1].

Blood irradiators are a critical safety measure in hospitals and blood banks, where they prevent transfusion-associated graft-versus-host disease (TA-GVHD). When donor white blood cells survive in a recipient, they may attack host tissue, with a mortality exceeding 90 % [2]. For irradiation of cellular blood products to effectively prevent TA-GVHD, the delivered dose must be high enough to suppress lymphocyte proliferation. [3] The RS 3400 (Rad Source Technologies) represents a shift from isotope-based to X-ray-based irradiation, employing a sealed gold-anode X-ray tube operated at approximately 150,155 kVp together with a mechanical rotator that moves the blood bags around the central tube to improve dose uniformity [4].

Monte Carlo (MC) simulation, particularly using platforms such as GATE (Geant4 Application for Tomographic Emission), has become a reference tool for modelling dose distributions in radiation physics. GATE is well suited to systems such as the RS 3400 because of its ability to represent complex geometries, time-dependent motion, and spatial dose scoring [5]. However, the fidelity of any simulation depends strongly on realistic geometry, source modelling, and the convergence of the statistical estimate. The aim of the present work is therefore to develop a complete GATE v9.0 model of the RS 3400 irradiator and to characterize, in detail, the simulated three-dimensional dose distribution within an ellipsoidal MAGIC-f gel blood-bag phantom, including the voxel-wise statistical uncertainty and a multi-level regional analysis of the dose uniformity that the rotating-canister design is intended to produce.

2 Related Work

Monte Carlo simulation has become an essential approach in radiation dosimetry because it allows absorbed dose to be estimated under complex irradiation conditions where direct measurement may be limited. In [6], reviewed the use of the GATE/Geant4 Monte Carlo platform for radiotherapy and dosimetry applications. They showed that GATE can model different radiation therapy scenarios and calculate three-dimensional absorbed dose distributions with statistical uncertainty, making it a flexible tool for dose calculation and treatment-related simulations.

Building on the importance of accurate dose estimation, in [7], investigated how scattering conditions affect dose delivery in preclinical irradiation. They developed a GATE-based Monte Carlo model of the Faxitron CP-160 irradiator and compared the simulation results with experimental measurements. Their results showed good agreement under reference conditions, with differences below 2%. However, when small phantom geometries were used, the lack of lateral scatter and backscatter caused dose differences greater than 15%. This indicates that standard dosimetry assumptions may not be accurate for small-volume irradiation setups.

While [7] focused on preclinical irradiation geometry, in [8], addressed dose verification in blood irradiators. They evaluated the dose distribution of a Gamma cell 3000 Elan blood irradiator using PAGAT gel dosimetry, TLD measurements, and Monte Carlo simulation. The results showed close agreement between the different methods, with

differences below 4%. This confirmed that PAGAT gel dosimetry is a reliable method for measuring three-dimensional dose distributions in blood irradiation systems

Moving from external blood irradiators to radionuclide-based irradiation, in [9], proposed a GATE/Geant4-based method to calculate absorbed dose coefficients for ex vivo blood samples irradiated with radionuclides in solution. Their model reproduced an 8 mL vial geometry and included several radionuclides commonly used in nuclear medicine. The results showed large radionuclide-dependent differences in absorbed dose coefficients, ranging from 10.23 $mGy \cdot mL \cdot MBq^{-1}$ for ^{99m}Tc to 15632.02 $mGy \cdot mL \cdot MBq^{-1}$ for ^{225}Ac.

After establishing absorbed dose coefficients, the same research direction was extended toward biological damage estimation. In [5], combined GATE/Geant4 with Geant4-DNA to estimate DNA double-strand breaks in lymphocyte nuclei after internal ex vivo irradiation. The simulated DNA damage agreed well with experimental data, with beta/gamma emitters producing approximately 0.012–0.016 $DSB \cdot cell^{-1} \cdot mGy^{-1}$. This study showed that Monte Carlo simulation can be used not only for absorbed dose calculation but also for linking dose with biological DNA damage.

Finally, in [10], applied the validated model to a wider set of 45 alpha- and beta/gamma-emitting radionuclides. Their results showed that beta/gamma emitters produced relatively low DSB yields, whereas alpha emitters produced denser DNA damage due to their higher linear energy transfer. The study also provided a useful database of S-values and DSB yields for future radiation protection and radiobiology studies.

Overall, these studies show a clear progression from general Monte Carlo dose calculation, to experimental validation of dose delivery, and finally to biological modelling of radiation-induced DNA damage. Together, they demonstrate that accurate dose estimation depends on irradiation geometry, scattering conditions, radionuclide type, and the biological target being investigated.

3 Problem Formulation and Methodology

This section describes the GATE Monte Carlo simulation of the RS 3400 blood irradiator. The model focuses on dose deposition in a MAGIC-f gel dosimeter phantom contained within a blood bag, irradiated by a 150 kV (10 mA) X-ray source over a 280 s protocol, with the goal of evaluating the spatial dose distribution and uniformity characteristics of the system.

3.1 Simulation Software and Hardware

The simulation was executed on a workstation with a 12th-generation Intel Core i9-12900K processor (16 cores), 64 GB of RAM, and 1.82 TB of storage. The software environment comprised Ubuntu 18.04 LTS, GATE v9.0 compiled with Geant4 10.6.1, SpekCalc v1.1 for spectrum generation, and MATLAB R2026a for data analysis. A structured directory framework was used to maintain reproducibility, comprising a macro directory (GATE command files), a data directory (the GateMaterials.db material database), and an output directory for the dose-actor results.

3.2 Materials and Geometry

3.2.1 Material database and coordinate system

Materials were defined through the GateMaterials.db database. The MAGIC-f gel was specified as a liquid of density 1.03 g/cm³ according the formula used in the simulation and effective atomic number 7.53, with an elemental composition (by mass) of oxygen 79.96 %, hydrogen 10.50 %, carbon 7.94 %, nitrogen 1.42 %, sulphur 0.17 %, and copper 0.0005 %. The simulation environment was a cubic world volume of 1 m per side, filled with air at standard conditions. The coordinate origin was placed at the world center, with the positive X-axis pointing toward the source, the Y-axis perpendicular to the beam, and the Z-axis vertical, forming a right-handed Cartesian system.

3.2.2 Lead-shielding assembly

A seven-component lead-shielding structure was implemented to reproduce realistic radiation-protection conditions. The central element was a cylindrical lead room positioned at the origin with an inner radius of 20 cm, an outer radius of 25 cm, and a height of 34 cm, providing a 5 cm thick barrier around a central cavity for the sample. Six rectangular lead boxes (each 5 × 55 × 55 cm) surrounded the cylinder along the ±X, ±Y, and ±Z directions to form a fully enclosed chamber. All lead components used a density of 11.34 g/cm³ (Z = 82). The resulting geometry is shown in Fig. 1.

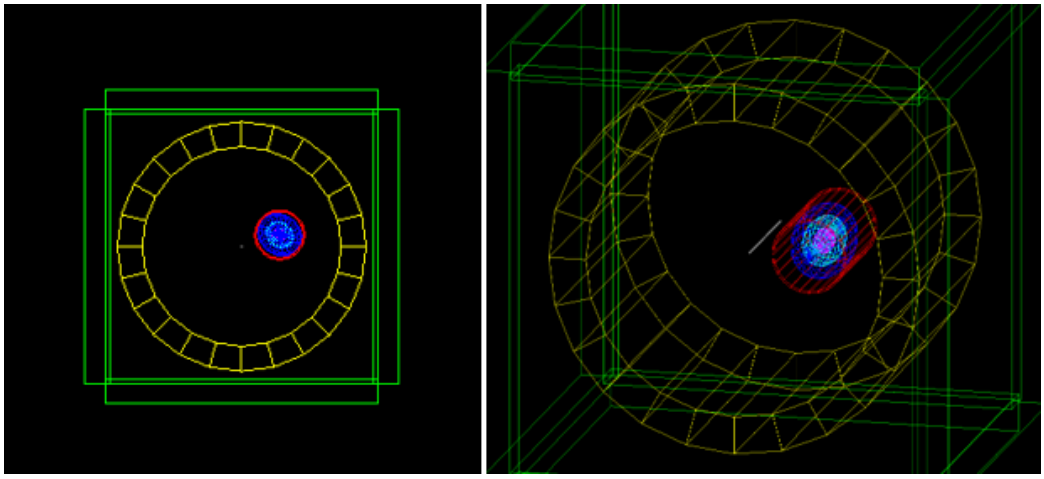

Fig. 1: GATE simulation geometry of the lead-shielding structure, showing the cylindrical lead room (yellow) surrounding the irradiation region and the six rectangular lead shields (green) enclosing the irradiation volume.

3.2.3 Blood container and ellipsoidal phantom

The blood container was modelled as a thin-walled cylinder of blood-equivalent material with an inner radius of 4.7 cm, an outer radius of 5.0 cm (3 mm wall), and a height of 17 cm, with its axis aligned along X and its center at (8, 0, 0) cm. The MAGIC-f gel itself was represented as a complete ellipsoid with semi-axes of 2.0 cm (X), 2.35 cm (Y), and 4.25 cm (Z), corresponding to full dimensions of 4.0 × 4.7 × 8.5 cm, approximating a partially filled blood bag positioned horizontally (Fig. 2). This geometry enables depth-dependent analysis of dose gradients from the surface to the core of the sample.

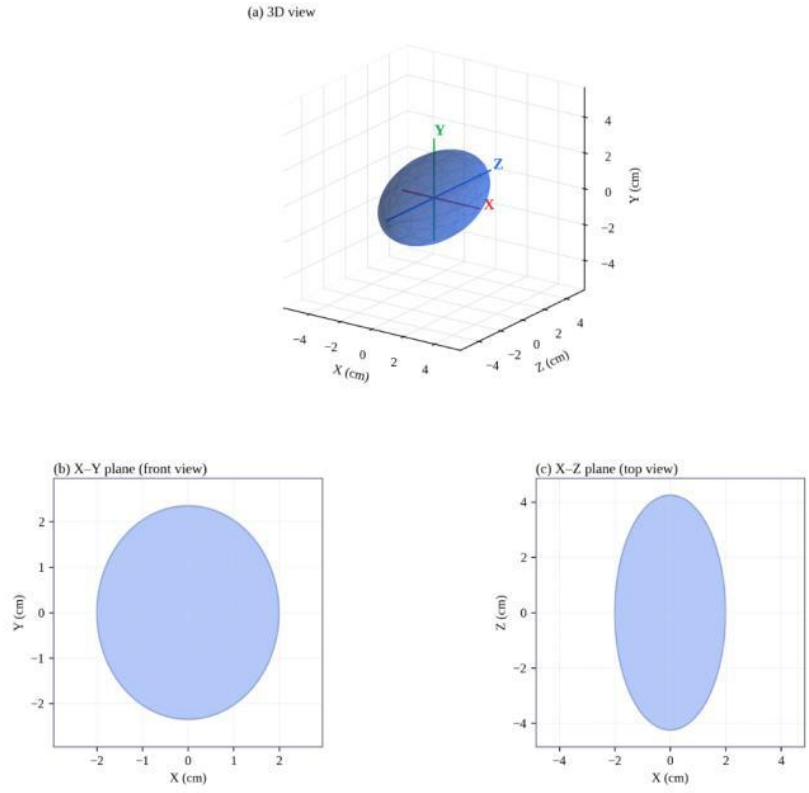

Fig. 2: Ellipsoidal model of the blood bag in GATE: (a) 3D view; (b) X–Y front projection; (c) X–Z top projection. Full extents 4.0 × 4.7 × 8.5 cm.

3.3 Source Modelling

3.3.1 Gold-anode X-ray spectrum

The RS 3400 employs a 150 kV gold-anode X-ray tube, which differs from conventional tungsten-based irradiators. Since a measured manufacturer-provided photon spectrum for the RS 3400 was not publicly available, the source spectrum used in this work was approximated using SpekCalc v1.1 as a baseline spectral model. SpekCalc was used to generate a filtered 150 kV tungsten-anode spectrum with 0.8 mm Be inherent filtration and 0.45 mm Cu additional filtration, as the software accounts for user-defined filtration materials and thicknesses. However, because SpekCalc is designed for tungsten-anode spectra, the resulting spectrum could not be assumed to directly represent the RS 3400 gold-anode output. Therefore, a first-order spectral modification was applied to approximate the gold-anode emission. The tungsten characteristic peaks at 57.98 keV (W Kα) and 67.24 keV (W Kβ) were removed and replaced with the principal gold characteristic peaks at 66.99 keV (Au $K\alpha_2$), 68.80 keV (Au $K\alpha_1$), and 77.98 keV (Au $K\beta_1$). The bremsstrahlung continuum was also adjusted using the atomic-number ratio between gold and tungsten ($Z_{Au}/Z_W = 79/74$), representing a simplified correction for the higher atomic number of gold. This approach should be regarded as an approximate reconstruction rather than a fully measured or manufacturer validated RS 3400 spectrum, since the exact spectral distribution also depends on tube geometry, anode self-attenuation, filtration, and angular emission characteristics. The final approximated spectrum was discretized into 32

energy bins spanning 10–150 keV, normalized to unit fluence, and used as the photon source distribution in the Monte Carlo simulation.

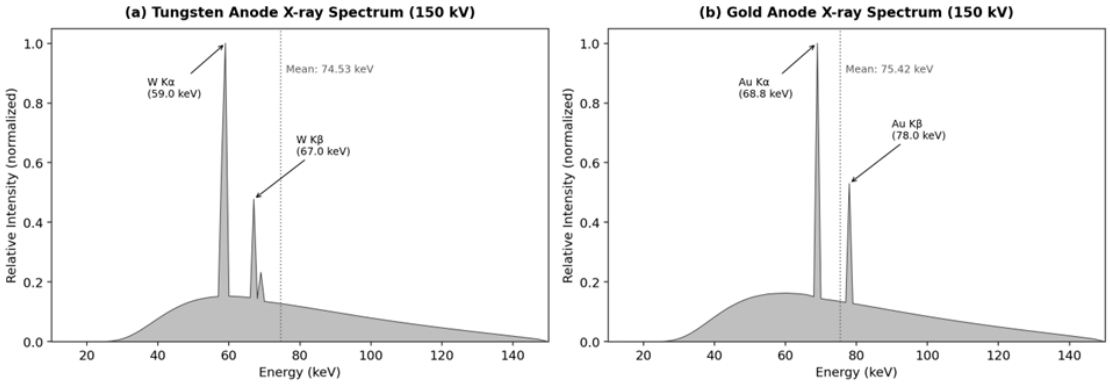

Fig. 3: (a) Original SpekCalc tungsten spectrum at 150 kV with 0.8 mm Be and 0.45 mm Cu filtration; (b) corrected gold-anode spectrum used as the GATE source input, with the tungsten peaks replaced by the Au Kα and Kβ peaks and the bremsstrahlung continuum scaled by the Z-ratio of 1.068. Both spectra are normalized to unit peak intensity.

3.3.2 Source geometry and intensity

The X-ray source was implemented as a vertical line source extending 17 cm along the Z-axis and centered at the origin, representing the elongated cylindrical gold-anode geometry of the second-generation RS 3400 tube. Photons were sampled uniformly in the azimuthal direction around the line source to approximate the 360-degree cylindrical emission of the tube. This approximation is consistent with the RS 3400 source concept [11], with the energy distributed proportionally to the spectral intensity at each bin. The tube current of 10 mA and irradiation time of 280 s correspond to a total charge of 2800 mAs; consequently, all dose outputs were multiplied by a post-processing factor of 2800 to scale the simulated dose to clinically relevant values.

3.4 Sample Motion and Time Discretization

To reproduce the dose-averaging effect of the physical rotator, two simultaneous motions were applied to the container and the gel phantom as a rigid assembly: a self-rotation of 6°/s about a vertical axis through the center of each component, and an orbital revolution of 3°/s about a vertical axis through the source at the origin. The 280 s exposure was divided into time slices of 0.01 s, giving 28000 time bins, so that the continuously moving geometry was tracked with high temporal fidelity. The simulation was performed using 10^{10} primary photons distributed uniformly over the exposure, using the MersenneTwister random-number generator with automatic seeding. This number is consistent with recent GATE-based Monte Carlo studies that have used photon histories of 10^{10}or less depending on the simulation geometry, scoring objective, and required uncertainty level. In [12] used 10^{10} primary photons per energy bin in GATE v9.2 simulations, while other recent GATE studies have used lower numbers such as 7×10^{9} [13] or 10^{8} [14] primaries when acceptable statistical precision was achieved.

3.5 Dose-Actor Configuration

Dose was scored using GATE dose actors on a 100 × 100 × 1 voxel grid positioned through the geometric centre of the gel. This scoring configuration was selected because the blood bag was centrally located within the irradiation container, and the combined rotational and orbital motion produces a near-symmetric irradiation geometry around the central region. At this central plane, the surrounding material thickness and source-to-sample geometry are expected to be most representative and least affected by boundary or end effects. Therefore, the high in-plane resolution in the X–Y direction was used to obtain a detailed coronal dose map at the region of primary interest, while the single voxel along the Z-direction restricted the analysis to the central plane where the geometry of the blood bag and container is most comparable during rotation. This approach focuses the dosimetric evaluation on the central region of the gel, where dose averaging from rotational motion is expected to be strongest and where dose homogeneity is most clinically relevant. Each dose actor recorded the deposited energy (MeV), the absorbed dose (Gy), and the voxel-wise statistical uncertainty. The uncertainty dose parameter was set to true, activating the native GATE/Geant4 statistical uncertainty calculation for each voxel in the dose distribution. The resulting uncertainty map provides a voxel-wise estimate of the statistical precision of the Monte Carlo dose scoring. In general, Monte Carlo uncertainty decreases with the number of particle histories and can be conceptually related to the standard error of the mean $\left(\sigma/\sqrt{N}\right)$, where σ represents the variation in dose contributions and Nrepresents the number of contributing histories. However, the uncertainty values reported in this study were obtained directly from the built-in statistical estimators implemented in GATE/Geant4, rather than being manually calculated using this simplified expression.

4 The Proposed Post-Processing Method

A unified MATLAB pipeline converted the raw GATE output, stored in MetaImage (.mhd/.raw) format, into absorbed-dose maps and performed the regional analysis. The pipeline imported the energy-deposition and uncertainty images, computed the voxel mass, converted energy to dose, generated a valid-dose mask, partitioned the masked region into concentric zones, and exported heatmaps, region maps, and statistical tables.

4.1 Energy-to-Dose Conversion

The voxel mass was obtained from the voxel volume and a literature-based MAGIC-f gel density of $\rho = 1030$ kg/m³ (the density of the prepared batch was not measured experimentally). The absorbed dose in each voxel was computed as:

$$D_{\mathrm{sim}}(x,y,z) = \frac{E_{\mathrm{dep}}(x,y,z)\times 1.602176634\times 10^{-13}}{\rho_{\mathrm{MAGIC-f}} V_{\mathrm{voxel}}} \quad (1)$$

where E_{dep} is the deposited energy in MeV, the factor 1.602×10^{-13} converts MeV to joules, and V_{voxel} is the voxel volume in m³. The converted dose could optionally be scaled to a nominal reference using the mean of the four central pixels; when no scaling was applied the analysis dose equals the converted dose.

4.2 Valid-Dose Mask and Regional Segmentation

To exclude background and very-low-dose regions, a binary analysis mask was generated using a threshold of 5% of the maximum dose, defined as $D_{th} = 0.05D_{max}$. This cutoff is consistent with recent dose-distribution validation work [15], where a 5% dose threshold was used during profile evaluation. The resulting mask was then refined by filling internal holes and removing small isolated components. The valid region was then partitioned with a distance transform d(p) measuring the distance of each pixel from the mask boundary. With $d_{\max}$ the maximum distance inside the mask, three concentric regions were defined as:

$$R_{\text{outer}} = \left\{p \in M: d(p) \leq \frac{d_{\max}}{3}\right\}$$
$$R_{\text{middle}} = \left\{p \in M: \frac{d_{\max}}{3} < d(p) \leq \frac{2d_{\max}}{3}\right\}$$
$$R_{\text{inner}} = \left\{p \in M: d(p) > \frac{2d_{\max}}{3}\right\} \quad (2)$$

The inner region was further subdivided by a second distance transform applied only within it, producing inner-outer, inner-middle, and inner-inner subregions using the same one-third / two-thirds partition. This allowed the central plateau to be examined at higher spatial resolution.

4.3 Regional Statistics

For each region R, percentile-based dose metrics were computed to assess dose homogeneity. The near-maximum dose $D_{5,R}$was defined as the dose received by the hottest 5% of pixels/voxels, while $D_{95,R}$represented the dose received by 95% of pixels/voxels. The dose homogeneity ratio was then calculated as the ratio of $D_{5,R}$to $D_{95,R}$:

$$\text{DUR}_R = \frac{D_{5,R}}{D_{95,R}} \quad (3)$$

The voxel-wise relative uncertainty was treated as a fraction and converted to a percentage, and the mean uncertainty was reported for each region. The same valid-mask generation, distance-transform segmentation, and statistical extraction were applied identically across all regions and to three manually drawn regions of interest (ROIs), ensuring a bias-free, multi-level characterization of the simulated dose distribution.

5 Results, Analysis and Discussions

5.1 Corrected Gold-Anode 150 kV Spectrum

The corrected gold-anode spectrum (Fig. 3b) exhibits a mean photon energy of 75.42 keV, slightly above the 74.53 keV mean of the underlying tungsten reference, owing to the higher-energy position of the gold characteristic lines. The strong copper filtration preferentially attenuates the low-energy bremsstrahlung below approximately 30 keV, producing an intentional beam-hardening effect that allows the RS 3400 to deliver a penetrating beam capable of acceptable dose uniformity through the full thickness of a blood bag. The spectral parameters are summarized in Table 1.

Table 1: Spectral parameters of the simulated X-ray beam used as the GATE source input.

Parameter	Value
Tube voltage	150 kV
Inherent filtration	0.8 mm Be
Additional filtration	0.45 mm Cu
Anode material	Gold (Z = 79)
Number of energy bins	32
Energy range	10 – 150 keV
Mean photon energy	75.42 keV
Peak photon energy (Au $K\alpha_1$)	68.80 keV
Characteristic peaks	66.99, 68.80, 77.98 keV

5.2 Coronal Dose Distribution

After the 280 s irradiation simulation, the GATE energy-deposition output was converted to absorbed dose by dividing the deposited energy in each voxel by the corresponding voxel mass, using the MAGIC-f gel density. Because the number of simulated primary photons is a computational parameter and does not directly correspond to the physical photon fluence produced during the 2800 mAs exposure, an absolute-dose normalization was applied during post-processing. The simulated dose distribution was scaled to the delivered irradiation condition using a reference-dose scaling factor, while preserving the relative spatial dose distribution predicted by the Monte Carlo calculation. After applying the 5% maximum-dose threshold to exclude background and very-low-dose voxels, the resulting central coronal dose map at 100×100×1 pixel resolution is shown in Fig. 4. The distribution shows a radial dose gradient, with the highest and most homogeneous dose region located near the geometric centre of the ellipsoidal gel volume and a gradual decrease toward the periphery. This behaviour is consistent with the expected dose averaging produced by the combined rotational and orbital motion of the irradiation canister..

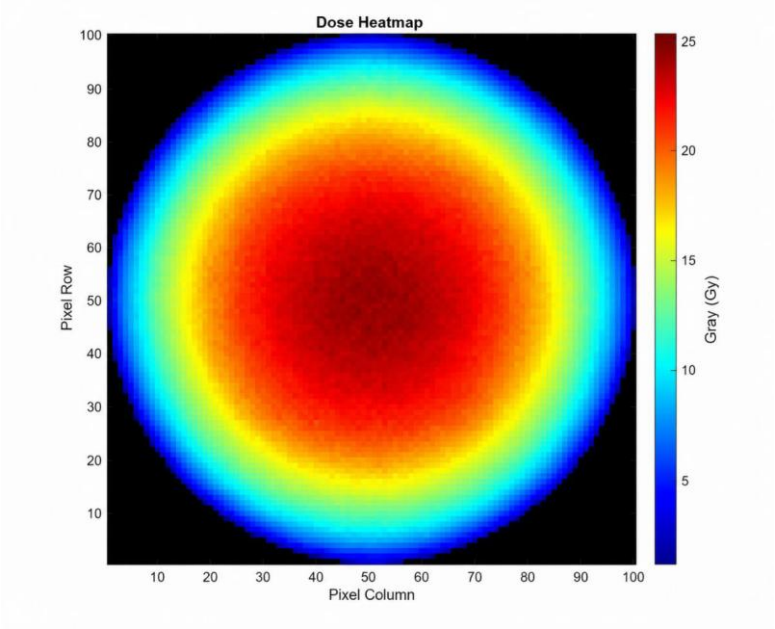

Fig. 4: Simulated absorbed-dose heatmap of the MAGIC-f gel blood-bag model in the coronal cross-section plane after conversion of the GATE energy-deposition output to absorbed dose.

5.3 Voxel-wise Statistical Uncertainty

The voxel-wise uncertainty map produced by the history method, after masking with the valid-dose mask, is shown in Fig. 5, and the summary statistics are given in Table 2. The mean statistical uncertainty within the valid mask was 0.771 %, with 96.3 % of voxels below 1 % and 98.8 % below 2 %. The uncertainty was highest at the periphery, where the contributing photon fluence is smallest, and lowest at the geometric canter, where the rotational and orbital motion improves dose averaging and dose homogeneity. These values confirm that the chosen 10^{10} primary histories and 0.01 s time slicing produced a converged dose estimate of clinically useful precision.

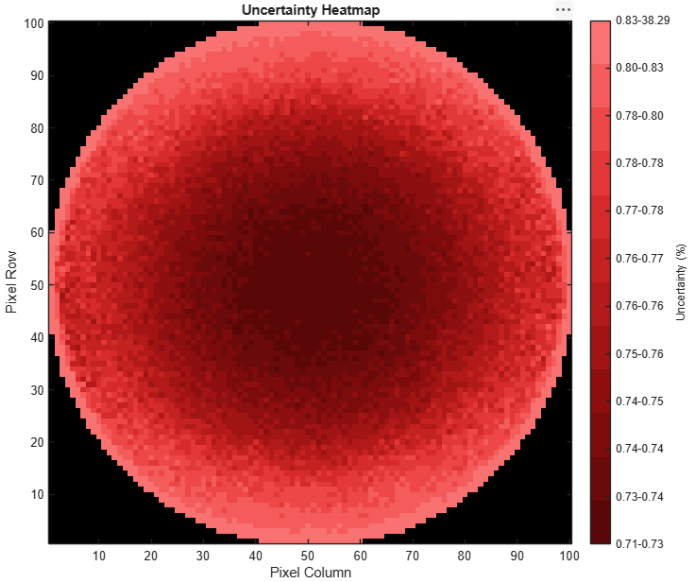

Fig. 5: Voxel-wise statistical uncertainty map of the simulated dose distribution in the coronal plane, expressed as a percentage, after application of the 5 % maximum-dose mask.

Table 2: Summary of the voxel-wise statistical uncertainty across the valid dose mask.

Quantity	Value (%)
Mean uncertainty	0.771
Maximum uncertainty	1.243
Minimum uncertainty	0.714
Standard deviation of uncertainty	0.049
Fraction of voxels with $\sigma \leq 1$ %	96.3
Fraction of voxels with $\sigma \leq 2$ %	98.8

5.4 Regional Dose Analysis

The valid mask was partitioned into outer, middle, and inner regions using the distance-transform segmentation of Section 4.2. The resulting region map and the dose heatmap with region boundaries are shown in Fig. 6, and the regional statistics are reported in Table 3. The inner region received the highest mean dose (23.92 Gy) and the outer region the lowest (10.66 Gy). The dose uniformity ratio improved markedly toward the center, from 4.78 in the outer region to 1.08 in the inner region, reflecting the higher local homogeneity of the central plateau.

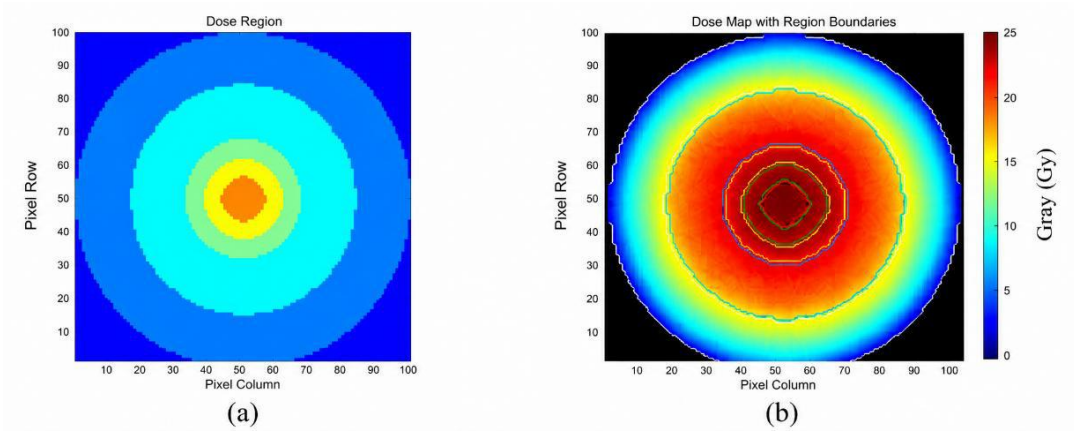

Fig. 6: (a) Distance-transform-based dose region map showing the division of the valid dose area into outer, middle, and inner regions. (b) Dose heatmap with the corresponding regional boundaries overlaid; the colour scale represents absorbed dose in Gy.

Table 3: Regional analysis of the simulated dose distribution within the outer, middle, and inner regions.

Region	N pixels	Mean dose (Gy)	σ_D (Gy)	D_{max} (Gy)	D_{min} (Gy)	DUR (D_5/D_{95})	Mean U (%)
Outer	4262	10.66	4.11	17.22	1.27	4.78	0.80
Middle	2632	20.04	1.74	23.29	16.62	1.31	0.75
Inner	920	23.92	0.58	25.34	22.63	1.08	0.73

5.5 Inner-Subregion Analysis

To examine the central plateau in more detail, the inner region was subdivided into inner-outer, inner-middle, and inner-inner subregions (Table 4). The innermost subregion received the highest and most uniform dose (mean 24.74 Gy, DUR = 1.03), confirming that the combined rotational and orbital motion promotes dose averaging, resulting in the most homogeneous dose distribution at the geometric center of the gel. The residual

relative dose gradient between the inner-outer and inner-inner subregions was small, providing a quantitative measure of the central dose non-uniformity.

Table 4: Inner-subregion analysis of the simulated dose distribution.

Subregion	N pixels	Mean dose (Gy)	σ_D (Gy)	D_{max} (Gy)	D_{min} (Gy)	DUR (D_5/D_{95})	Mean U (%)
Inner-outer	480	23.45	0.34	24.20	22.63	1.05	0.729
Inner-middle	312	24.30	0.27	24.94	23.48	1.04	0.724
Inner-inner	128	24.74	0.21	25.34	24.27	1.03	0.720

5.6 ROI-Based Analysis

Three user-defined ROIs were drawn at the geometric center, a middle position, and a peripheral position near the surface (Fig. 7), each restricted to the valid mask. The ROI statistics (Table 5) reproduce the spatial trend of the regional analysis: the central ROI received the highest and most uniform dose (24.91 Gy, DUR = 1.03), the middle ROI received an intermediate dose (16.94 Gy, DUR = 1.12), and the peripheral ROI received the lowest dose (8.50 Gy, DUR = 1.29). This confirms that the spatial features of the global dose map are preserved even when the dose is averaged over small, manually selected areas.

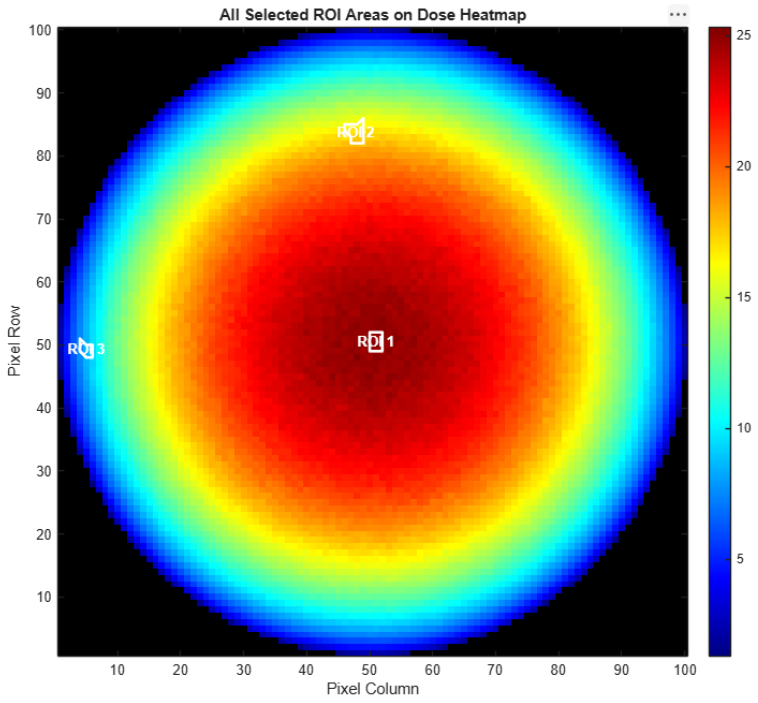

Fig. 7: Spatial distribution of the absorbed dose with three regions of interest marked: ROI 1 in the central high-dose region, ROI 2 in an intermediate-dose region, and ROI 3 near the low-dose outer region.

Table 5: ROI-based statistics of the simulated dose distribution at three selected locations.

ROI	Mean dose (Gy)	σ_D (Gy)	D_{max} (Gy)	D_{min} (Gy)	DUR (D_5/D_{95})	Mean U (%)
ROI-1 (Center)	24.91	0.21	25.22	24.53	1.03	0.720
ROI-2 (Middle)	16.94	0.66	17.90	15.83	1.12	0.766
ROI-3 (Peripheral)	8.50	0.88	9.59	7.43	1.29	0.767

5.7 Discussion

The simulation results indicate that the developed GATE model reproduces the expected dosimetric behaviour of the RS 3400 at the 150 kV / 10 mA / 280 s operating point. The inner-region mean dose of 23.92 Gy is consistent with the nominal 25 Gy target for blood-product irradiation, and the inner-region uniformity ratio of 1.08, together with the inner-inner value of 1.03, demonstrates that the combined motion effectively homogenizes the central dose. This is direct evidence that the time-discretized motion model 28 000 slices of 0.01 s each correctly reproduces the dose-averaging effect of the physical sample motion: in a static configuration, the side of the phantom facing the source would receive a substantially higher dose than the opposite side, whereas the rotating model yields a near-unity central uniformity ratio.

The mean voxel-wise uncertainty of 0.771 %, with more than 96 % of voxels below 1 %, confirms statistical convergence sufficient for the multi-level analysis. The strong copper filtration and the resulting mean energy of 75.42 keV explain the penetrating character of the beam and the broad central plateau. The consistency among the global, regional, inner-subregion, and ROI analyses all reproducing the same center-to-periphery gradient provides an insight of the post-processing pipeline and indicates that the model can serve as a reliable dosimetric surrogate of the RS 3400 in the central high-dose region. A current limitation is the use of a post-processed, rather than directly simulated, gold-anode spectrum and a literature-based gel density; both introduce small systematic uncertainties that are candidates for refinement in future work, alongside experimental validation with polymer-gel dosimetry.

6 Conclusion

A complete GATE v9.0 Monte Carlo model of the RS 3400 X-ray blood irradiator was developed and characterized at the 150 kV / 10 mA / 280 s operating point. The model incorporates a corrected gold-anode 150 kV spectrum (mean energy 75.42 keV, 32 energy bins), a seven-component lead-shielding assembly, an ellipsoidal MAGIC-f gel blood-bag phantom, and a combined self-rotation (6°/s) and orbital revolution (3°/s) implemented through 28 000 time slices with 10^{10} primary photons. A unified MATLAB pipeline converted the energy-deposition output to absorbed dose and performed voxel-wise uncertainty, regional, inner-subregion, and ROI-based analyses in the coronal plane.

The simulated distribution exhibits a homogeneous central plateau (inner-region mean 23.92 Gy, inner-region DUR 1.08, and inner-inner mean 24.74 Gy with DUR 1.03) decreasing radially toward the periphery, with a mean statistical uncertainty of 0.771%. These results confirm that the combined motion model homogenizes the central dose and that the simulation is converged to a clinically useful precision. Future work will replace the post-processed spectrum with a direct Monte Carlo simulation of the gold target, use an experimentally measured gel density, extend the comparison to a full three-dimensional volumetric analysis, and validate the model experimentally against MAGIC-f polymer-gel measurements across the full clinical operating envelope.

7 Future work

Although the present model reproduces the central dose plateau of the RS 3400 with clinically useful precision, several open problems remain before a Monte Carlo model can be adopted as a fully traceable dosimetric reference for non-isotopic X-ray blood irradiators. The principal open problem is the establishment of an absolute, experimentally anchored dose scale: the dose reported here is a nominal absolute distribution derived from the tube charge and a literature-based gel density, and a machine-specific experimental dosimetry report is required to convert it into a traceable absolute dose. Resolving this would allow the model to be used directly for routine dose validation rather than as a relative spatial reference.

At the level of the source model, the gold-anode spectrum was obtained by post-processing a SpekCalc tungsten reference rather than by a direct simulation of the X-ray tube. A natural extension is to replace this approximation with a full Monte Carlo simulation of the gold target, the inherent and additional filtration, and the tube housing, which would remove the residual uncertainty in the characteristic-peak intensities and in the bremsstrahlung scaling. In parallel, the MAGIC-f gel density, assigned here a literature value of 1.03 g/cm^3, should be measured for each prepared batch so that the energy-to-dose conversion uses the actual rather than an assumed density.

The dosimetric characterization was performed in the coronal (Y = 0) plane only. A full three-dimensional volumetric comparison, obtained by acquiring orthogonal coronal, sagittal, and axial planes, would provide a more complete validation of the simulated dose volume. Such validation introduces a further open problem specific to gel dosimetry: the semi-liquid MAGIC-f gel deforms when the flexible blood bag is removed from the rigid container for imaging, so that the measured spatial dose pattern no longer coincides with the rigid simulation geometry. Future experiments should therefore either image the gel while it remains constrained in a rigid holder that reproduces the irradiation geometry, or incorporate a deformable image-registration step that maps the measured dose back onto the simulation geometry.

Finally, the model has so far been validated at a single operating point (150 kV / 10 mA / 280 s). Applying it across the full range of tube currents, irradiation times, and motion settings would characterize the dosimetric response over the complete clinical operating envelope and support optimization of the dose uniformity. Building on this, a practical quality-assurance protocol could be developed in which routine verification of the RS 3400 output is performed by comparison against the validated model together with a small number of MAGIC-f gel measurements, reducing the need for a full physical dosimetry survey at each verification.

ACKNOWLEDGEMENTS

The authors gratefully acknowledge the Nuclear Engineering Department, Faculty of Engineering, King Abdulaziz University, for providing the computational resources and technical support used in this work.

Bibliography

[1] K. Soliman, M. Adili and A. Alrushoud, "Radiation dose verification of an X-ray based blood irradiator using EBT3 radiochromic films calibrated using Gamma Knife machine," *Reports of Practical Oncology and Radiotherapy,* vol. 24, pp. 369 - 374, 2019.

[2] i. b. Australian & New Zealand Society of Blood Transfusion, Guidelines for the prevention of transfusion-associated graft-versus-host disease (TA-GVHD), Sydney, NSW: Australian & New Zealand Society of Blood Transfusion , 2024 .

[3] B. H. S. a. C. D. H. a. J. S. a. M. R. Gil, "Chapter 49 - Irradiation of Blood Products," in *Transfusion Medicine and Hemostasis (Fourth Edition)*, Elsevier, 2025, pp. 229-232.

[4] I. Rad Source Technologies, "RS 3400 Operator's Manual," Rad Source Technologies, Inc, Buford, GA, 2019.

[5] D. Sarrut, M. Bardiès, . N. Boussion, . N. Freud, S. Jan, J.-M. Létang, G. Loudos, L. Maigne, . S. Marcatili and et al., " A review of the use and potential of the GATE Monte Carlo simulation code for radiation therapy and dosimetry applications," *Medical Physics,* vol. 41, no. 6, p. 064301, 2014.

[6] M. Salas-Ramirez, M. Lassmann and U. Eberlein, "In silico analysis of radiation-induced double-strand breaks by internal ex vivo irradiation of lymphocytes for 45 alpha-and beta/gamma-emitting radionuclides," *EJNMMI research,* vol. 15, p. 21, 2025.

[7] M. Salas-Ramirez, L. Michael and U. Eberlein, "GATE/Geant4-based dosimetry for ex vivo in solution irradiation of blood with radionuclides," *Zeitschrift für Medizinische Physik,* vol. 33, p. 46–53, 2023.

[8] P. Mohammadyari, M. Zehtabian, S. Sina, A. R. Tavasoli and R. Faghihi, "Dosimetry of gamma chamber blood irradiator using PAGAT gel dosimeter and Monte Carlo simulations," *Journal of Applied Clinical Medical Physics,* vol. 15, p. 317–330, 2014.

[9] M. Salas-Ramirez, L. Maigne, G. Fois, H. Scherthan, M. Lassmann and U. Eberlein, "Radiation-induced double-strand breaks by internal ex vivo irradiation of lymphocytes: Validation of a Monte Carlo simulation model using GATE and Geant4-DNA," *Zeitschrift für Medizinische Physik,* vol. 35, p. 235–247, 2025.

[10] C. Noblet, S. Chiavassa, F. Paris, S. Supiot, A. Lisbona and G. Delpon, "Underestimation of dose delivery in preclinical irradiation due to scattering conditions," *Physica Medica,* vol. 30, p. 63–68, 2014.

[11] I. Rad Source Technologies, "510(k) Summary: RS 3400 Rad Source X-ray Blood Irradiator, K082921," U.S. Food and Drug Administration, Alpharetta, GA, 2009.

[12] G. Roque, M. L. Pérez-Lara, S. Cely , J. S. U. Parra, J. D. Bermúdez , M. K. Schütz, M. Fiederle , C. Ávila and S. Procz , "Energy-Resolved CNR Performance in Dense-Breast and Implant X-Ray Mammography Using a CdTe Photon-Counting Detector: A Monte Carlo Study," *Applied Sciences,* vol. 16, 2026.

[13] G. Savvidis, V. Eleftheriadis, V. Paneta, E. Fysikopoulos, M. Georgiou, E. Lamprou, S. Lagoumtzi, G. Loudos, P. Katsakiori and G. C. Kagadis, "Design and Evaluation of a Portable Pinhole SPECT System for 177Lu Imaging: Monte Carlo Simulations and Experimental Study," *Diagnostics,* vol. 15, p. 1387, 2025.

[14] S. Blind, L. Lerouge, M. Gries, P. Retif, N. Thomas, M. Barberi-Heyob and J. Daouk, "An alternate model to describe the radio-potentializing effects of metal-based nanoparticles in radiation therapy," *Computers in Biology and Medicine*, vol. 188, p. 109861, 2025.

[15] S. D. Rusu, B. R. Smith, G. H. Hutchinson, J. H. Jen and D. E. Hyer, "Commissioning and validation of the Elekta One GPUMCD algorithm for an Elekta VersaHD linear accelerator," *Journal of Applied Clinical Medical Physics,* vol. 27, p. e70540, 2026.